JMEPEG (2016) 25:2993–3006
DOI: 10.1007/s11665-016-2124-2

1059-9495/$19.00

Wear Resistance of H13 and a New Hot-Work Die Steel at High temperature

Shuang Li, Xiaochun Wu, Shihao Chen, and Junwan Li

(Submitted December 16, 2015; in revised form April 19, 2016; published online May 20, 2016)

The friction and wear behaviors of a new hot-work die steel, SDCM-SS, were studied at high temperature under dry air conditions. The wear mechanism and microstructural characteristics of the SDCM-SS steel were also investigated. The results showed that the SDCM-SS steel had greater wear resistance compared with H13 steel; this was owed to its high oxidizability and temper stability. These features facilitate the generation, growth, and maintenance of a tribo-oxide layer at high temperature under relatively stable conditions. The high oxidizability and thermal stability of the SDCM-SS steel originate from its particular alloy design. No chromium is added to the steel; this ensures that the material has high oxidizability, and facilitates the generation of tribo-oxides during the sliding process. Molybdenum, tungsten, and vanadium additions promote the high temper resistance and stability of the steel. Many fine Mo_2C and VC carbides precipitate during the tempering of SDCM-SS steel. During sliding, these carbides can delay the recovery process and postpone martensitic softening. The high temper stability postpones the transition from mild to severe wear and ensures that conditions of mild oxidative wear are maintained. Mild oxidative wear is the dominant wear mechanism for SDCM-SS steel between 400 and 700 °C.

Keywords hot-work die steel, microstructure, oxidative wear, wear resistance

1. Introduction

Hot-work die steels are widely used in manufacturing industries, for applications such as hot forging and press hardening, where the steels endure high temperatures and mechanical loads (Ref 1-4). In these applications, the main failure mechanism of the die is wear, especially high-temperature oxidative wear. This is the predominant wear mechanism for the majority of engineering parts subjected to high temperature (Ref 1, 5-11). Oxidative wear occurs frequently when steel is subjected to high temperature. Quinn et al. (Ref 12, 13) first proposed the model of oxidative wear. Archard et al. (Ref 14) researched the relationship between the tribo-oxide layer and wear, and proposed classifications of mild and severe wear. Hsu et al. (Ref 15) categorized the oxidative wear of metal into mild and severe oxidative wear. Under mild oxidative wear conditions, the wear rate is relatively low. However, under severe oxidative wear conditions, the wear rate is high, which may lead to premature wear failure of the hot-work die. Therefore, severe oxidative wear should be limited or avoided during the service life of hot-work die steel. Under harsh conditions, the transition from mild to severe wear often occurs because of dry sliding friction, particularly at high temperature (Ref 16-19). Controlling and avoiding the transition from mild to severe oxidative wear has great theoretical significance for engineering applications involving steel and iron materials.

A number of researchers found that high-temperature friction and wear behaviors are closely related to the tribo-oxide layer and matrix (Ref 3, 10, 12, 13, 16, 20, 21) of the material. The wear rate is reduced when the matrix is maintained at a specific strength that supports the tribo-oxide layer. Mild oxidative wear behavior is closely related to the degree of tribo-oxidation, as well as the thickness of the tribo-oxide layer. A number of studies have demonstrated that the wear behavior and wear rate depend on tribo-oxidation, rather than the microstructure of the steel matrix (Ref 22-24). However, when significant softening occurs in the substrate beneath the oxide at high temperature, conditions of mild oxidative wear will not be maintained (Ref 25). Wang et al. (Ref 20) demonstrated that asperity contact mechanics dominate the wear process under conditions of mild wear, while plastic deformation of the matrix is dominant under conditions of severe wear. Steels with high oxidizability can easily form oxides and tribo-oxide layers during sliding. Meanwhile, properties of high strength and hardness are maintained for steels with high temper stability; consequently, large plastic deformation is avoided and the tribo-oxide layer is preserved. Therefore, conditions of mild oxidative wear can be maintained for steels with high temper stability and oxidizability; this promotes high wear resistance.

The purpose of this work is to study the friction and wear behaviors of a new hot-work die steel, known as SDCM-SS, at high temperature. This work can provide a reference for the development and efficient utilization of hot-work die steel.

2. Experimental Procedure

2.1 Materials and Heat Treatment

AISI H13 steel is a conventional Cr-Mo-V-type hot-work die steel, which is used to produce hot-press casting and forging

Shuang Li, Xiaochun Wu, Shihao Chen, and **Junwan Li**, State Key Laboratory of Advanced Special Steel, Shanghai University, Shanghai 200072, China; Shanghai Key Laboratory of Advanced Ferrometallurgy, Shanghai University, Shanghai 200072, China; and School of Materials Science and Engineering, Shanghai University, Shanghai 200072, China. Contact e-mail: pirateshuang@shu.edu.cn.

dies. However, owing to its low wear resistance at high temperature, H13 steel is unsuitable for use under certain harsh working conditions. Therefore, a new Mo-W-V-type hot-work die steel, known as SDCM-SS, has been developed with excellent wear performance at high temperature. Table 1 shows the compositions of the SDCM-SS steel and commercial AISI H13 steel.

2.2 Tempering Tests

The specimens used for the tempering tests had dimensions of $10 \times 10 \times 20$ mm. The SDCM-SS steel samples were austenitized for 45 min at a temperature of 1080 °C while the H13 steel samples were austenitized for 30 min at a temperature of 1030 °C. Subsequently, all the samples were quenched in oil. Finally, the samples were tempered twice at 450, 500, 520, 540, 560, 580, 600, 620, 640, and 660 °C for 2 h. Following tempering, the hardness of the samples was measured using a Rockwell hardness tester (Leco R-260).

2.3 Temper Stability Test

The specimens used for the temper stability tests had dimensions of $10 \times 10 \times 20$ mm. The initial heat-treatment process is described in the following paragraphs. First, the SDCM-SS steel samples were austenitized at 1080 °C for 45 min, quenched in oil, and then tempered twice at 635 °C for 2 h. This resulted in a hardness value of 53 ± 0.4 HRC. The H13 steel samples were austenitized at 1030 °C for 30 min, quenched in oil, and then tempered twice at 520 °C for 2 h. This resulted in a hardness value of 52.8 ± 0.6 HRC. Finally, samples of the two steels were also tempered at 650 °C for periods ranging from 1 to 24 h.

2.4 High-Temperature Oxidation Test

The oxidizability of steel has an important role in determining its oxidative wear. In this work, static oxidation tests were performed on SDCM-SS and H13 steels within an S2-5-12-type resistance furnace at temperatures of 500 and 700 °C for 1, 3, 7, and 10 h, under dry air conditions. The samples used for the static oxidation tests had dimensions of $10 \times 10 \times 10$ mm. First, these samples were ground and polished with 600 grit silica carbide (SiC) abrasive paper using a polishing machine at a rotational speed of 600 r/min. Subsequently, prior to oxidation testing, they were washed with ethanol and dried. The surface roughness (Ra) of the polished sample was approximately 0.209 μm. Oxidation resistance is evaluated by the weight gain rate after oxidation testing. The weight gain rate, W, is calculated using the formula $W = (W_i - W_0)/S$, where W_0 and W_i are the weights of the samples (mg) before and after the oxidation test, respectively. S denotes the superficial area (mm^2).

2.5 Wear Test

To study the wear resistance of the SDCM-SS and H13 hot-work die steels, the initial heat treatment performed on the wear test sample was identical to that performed on the tempering stability test sample. The plate sample had dimensions of $10 \times 10 \times 35.5$ mm. Following the heat treatment, the samples were ground to remove the oxide layer, and subsequently cleaned with ethanol and air dried. They were then fixed on a drive in the heating chamber prior to the test. Ball-on-plate reciprocating dry sliding wear tests were conducted using a UMT-3 high-temperature wear tester; a schematic of the wear tester is shown in Fig. 1. The ball material consisted of SiC ceramic. The ball had a diameter of 9.525 mm and its hardness was 2800 HV at room temperature. The ball was installed in a holder prior to the test, and the sample was installed on a driver. During the test, the SiC ceramic ball slides upon the SDCM-SS and H13 steel plate samples in a linear reciprocating motion. A vertical downward load was applied to the flat samples via the ball. Table 2 shows the test parameters of the wear test. The wear rate, W_R, is calculated by the equation $W_R = V/NL$, where V is the wear volume (mm^3), N is the load (N), and L is the sliding distance (m). The wear volumes were measured using an optical profilometer (ContourGT-K1, Bruker Company, USA). The average values obtained from two or three samples are presented.

2.6 Observation of Microstructure and Worn Surface

The microstructures of the steels were examined using a scanning electron microscope (SEM, ZEISS Supra40 type, Germany) and transmission electron microscope (TEM, JEOL2010F, Japan) equipped with an energy dispersive spectral (EDS) analyzer under an operating voltage of 200 kV. For the TEM examination, thin foil samples were cut, ground, and subsequently dimpled via final ion thinning using a double-jet electro polisher at low temperature. The morphology, composition, and microstructure of the worn surface and subsurface were examined by SEM. The Vickers hardness values were measured at least five positions using a digital microhardness tester (MH-3, China), and the average values are presented.

3. Results and Discussion

3.1 Microstructure

Figure 2 shows the tempering hardness curves of the tested steels. The SDCM-SS steel exhibits secondary hardening, which results from the precipitation of alloy carbides in the tempered martensite. A pronounced secondary-hardening peak is presented at 600 °C. The microstructures of the tempered SDCM-SS steel consist of the martensite matrix and scattered primary and secondary carbides. Figure 3(a) shows a TEM image of spherical MC-type vanadium-rich carbides while Fig. 3(b) presents a TEM image of M_6C-type molybdenum and tungsten-rich carbides. Owing to the secondary carbides that precipitate from the martensite matrix, the softening effect is reduced, and therefore the hardness of the steel will increase

Table 1 Compositions of tested steels (wt.%)

	C	Si	Mn	Cr	(Mo + W)	V	P	S	Fe
H13	0.38	1.0	0.50	5.50	1.50	0.90	0.01	0.01	Balance
SDCM-SS	0.48	0.10	0.08	…	4.87	0.91	0.01	0.01	Balance

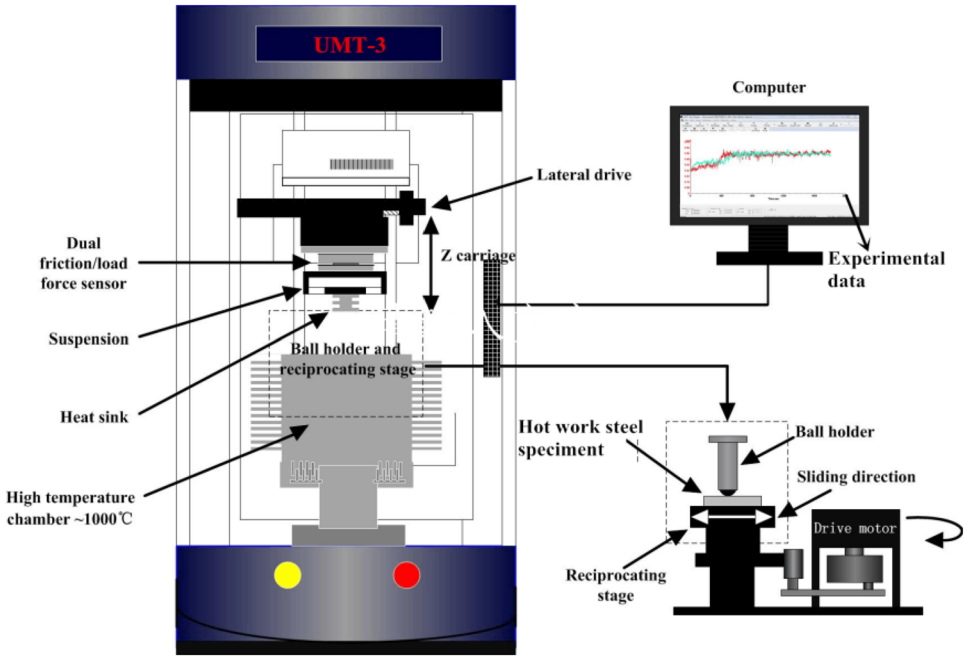

Fig. 1 Schematic diagram of the wear tester

Table 2 The summary of the wear test parameters

Temperature, °C				Load, N	Frequency, Hz	Velocity, m/s	Distance, m
400	500	600	700	10	5	0.1	360

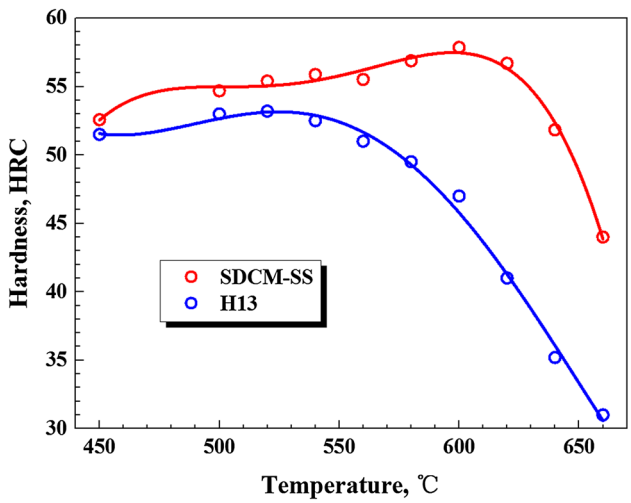

Fig. 2 The tempering hardness curves for various tempering temperatures of tested steels

during the tempering process. In SDCM-SS steel, the key elements associated with secondary hardening and tempering resistance are vanadium and molybdenum. During tempering, vanadium and molybdenum precipitate as very fine particles consisting of vanadium-rich MC carbides and molybdenum-rich M_2C carbides, respectively. Compared with vanadium and molybdenum, tungsten is less able to form carbides, and therefore, primarily functions in the solid solution strengthening of SDCM-SS steel. Figure 3(c, d) and (e-f) shows a bright-field TEM image, dark-field TEM image, and diffraction patterns of the secondary VC and Mo_2C carbides in the tempered SDCM-SS steel, respectively. Vanadium and molybdenum are the main alloying elements of the SDCM-SS steel. They are strong carbide-forming elements and have a strong secondary-hardening effect. A great number of Mo_2C and VC carbides precipitate in the SDCM-SS steel during tempering. These carbides, which possess relatively high hardness and thermal endurance, will affect the mechanical properties of hot-work die steel at high temperature. As a fairly stable carbide, VC will start to coarsen at 700 °C (Ref 26).

3.2 Temper Stability

Figure 4 shows the hardness curves of the steels that were tempered at 650 °C for various periods. The SDCM-SS steel shows superior temper stability compared with the AISI H13 steel. Following holding at 650 °C for 24 h, the hardness of the SDCM-SS steel was approximately 18 HRC greater than that of the H13 steel. In addition, the microstructure of the SDCM-SS steel consisted of tempered sorbite and had a high hardness (42 HRC). The relatively small size of the carbides of the SDCM-SS steel was maintained. In contrast, the microstructure of the H13 steel consisted of a ferrite matrix with some relatively large granular carbides, and had a lower hardness of 25 HRC, as shown in Fig. 5.

During tempering, the recovery of martensitic steel involves the precipitation and coarsening of carbides, as well as the rearrangement of dislocations inherited from quenching (Ref 27, 28). With regard to long-term tempering, the temper resistance of the steel strongly depends on the

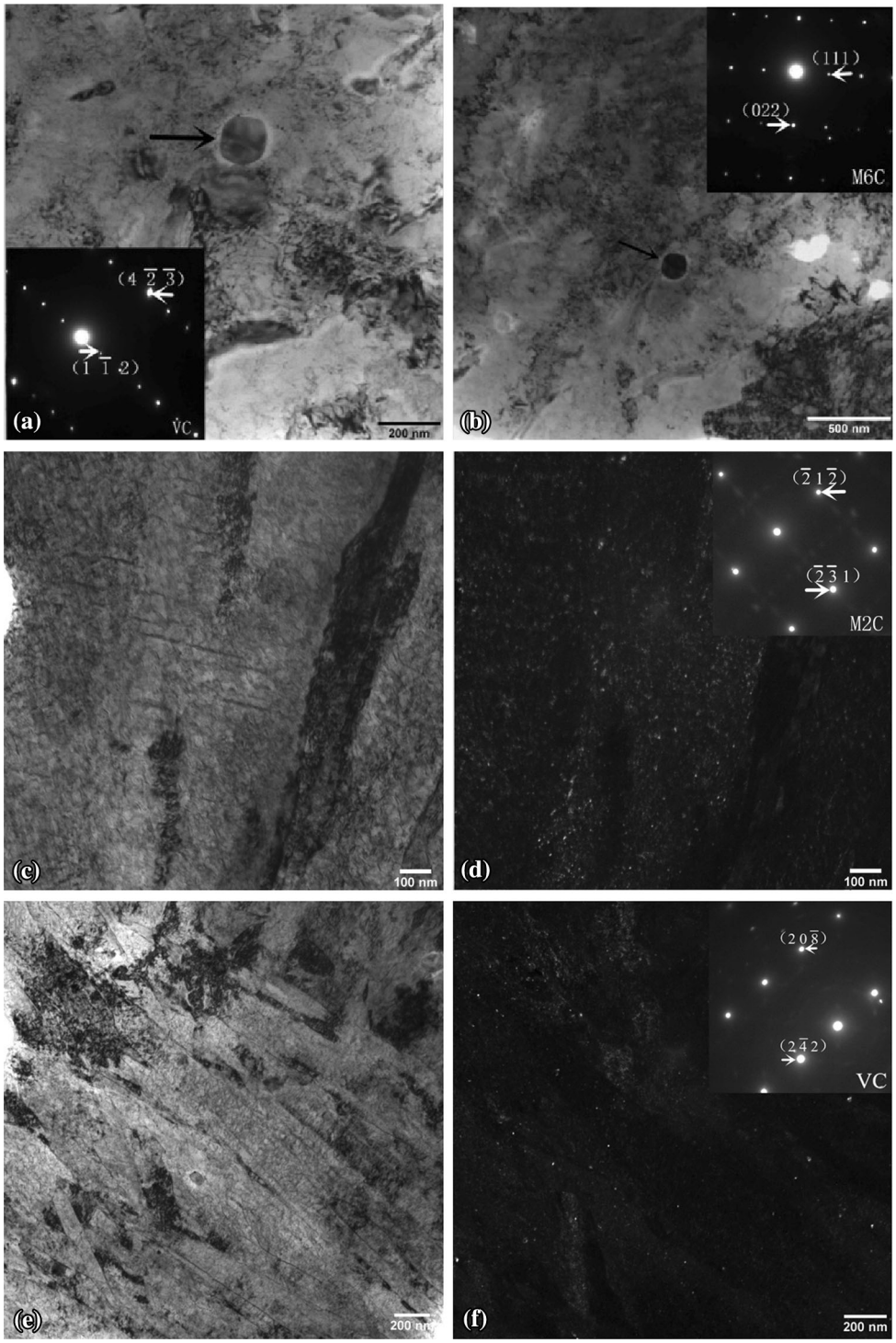

Fig. 3 TEM micrographs of bright image of (a) VC and M6C (b) carbides, (c) bright- and (d) dark-field images of M2C carbide, (e) bright- and (f) dark-field images of VC secondary carbide in SDCM-SS steel

over-aging resistance of the carbides. Fine carbides can prevent rapid recovery because they impede the motion of dislocations (Ref 29, 30). Many Mo_2C and VC carbides precipitated in SDCM-SS steel during tempering. These carbides, with greater size stability at high temperature, hinder dislocation glide and postpone martensite softening. Therefore, tempered SDCM-SS steels possess great high-temperature temper stability.

3.3 High-Temperature Oxidation

Oxides have a remarkable influence on the friction and wear behavior of steels and alloys (Ref 31). The weight gain rate associated with oxidation can be used as an indicator to assess the oxidizability of steel (Ref 32). Curves showing the oxidation weight gain as a function of time at 500 and 700 °C are presented in Fig. 6(a) and (b). The quantity of oxide

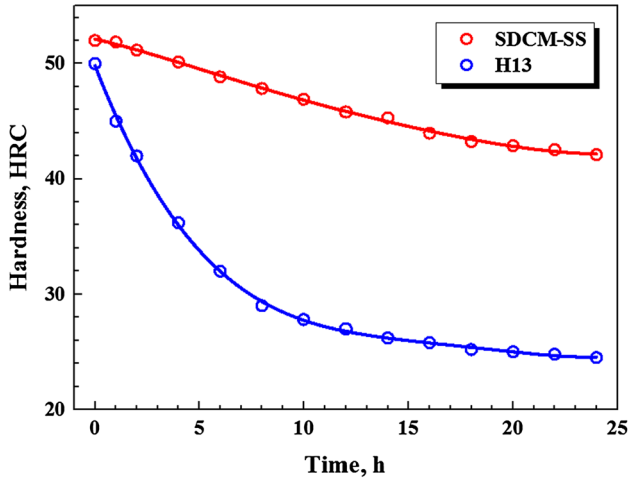

Fig. 4 The hardness curves for various tempering time of tested steels at 650 °C

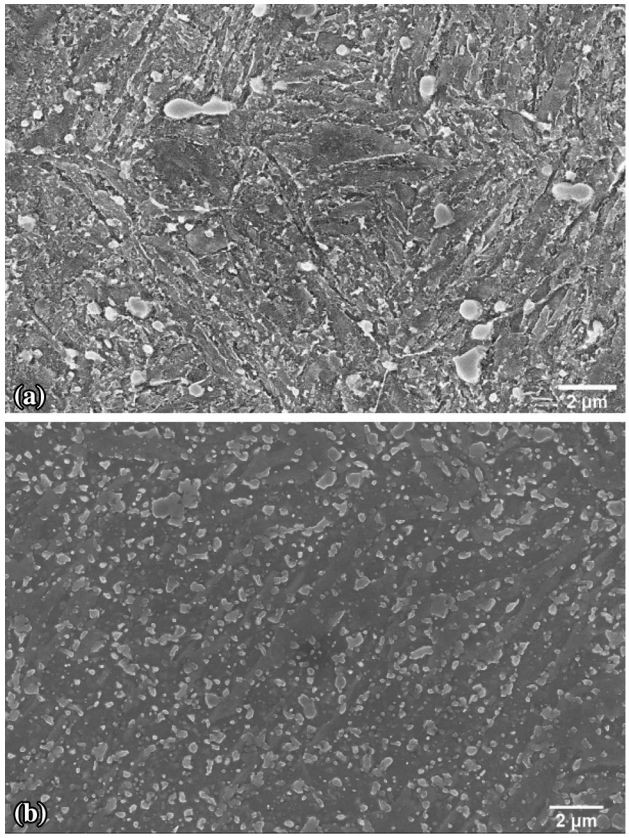

Fig. 5 Microstructure of (a) SDCM-SS and (b) H13 steels after tempered 24 h at 650 °C

increases as the temperature is increased and holding time is extended. The SDCM-SS steel exhibits more violent oxidation and its weight gain is approximately twice that of H13 steel. It is clear that steel with a greater Cr content exhibits greater oxidation resistance and produces fewer oxides. The oxidation resistance of steel increases as the Cr content increases, which directly affects the degree of oxidation under certain conditions. Therefore, the SDCM-SS steel, with no Cr content, exhibits greater oxidizability compared with the H13 steel.

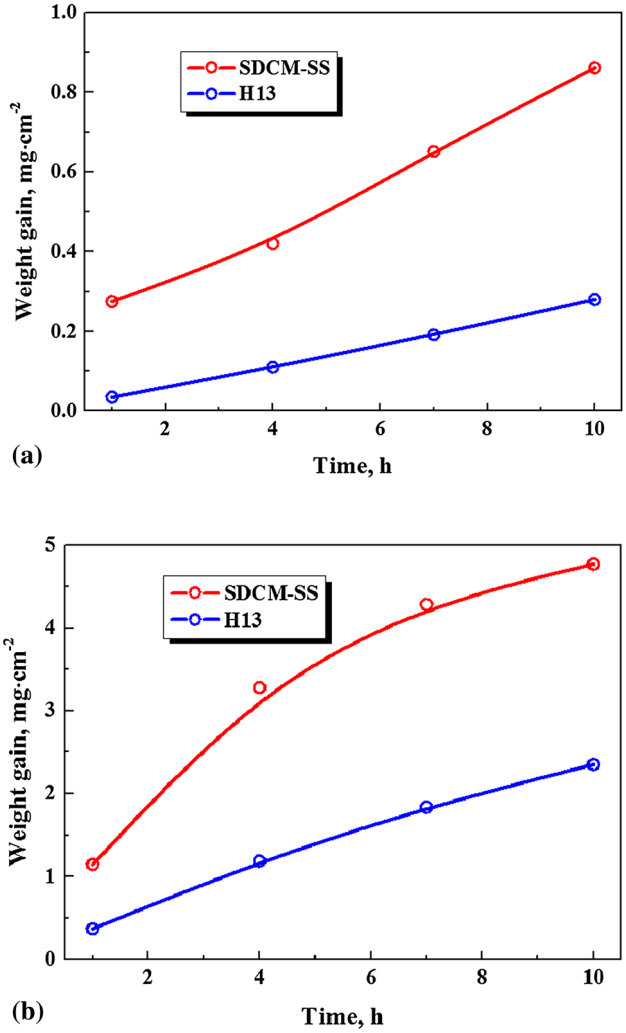

Fig. 6 The weight gain curves for various holding time of tested steels at (a) 500 °C and (b) 700 °C

3.4 High-Temperature Friction and Wear Behaviors

Figure 7 shows the wear rates of the SDCM-SS and H13 steels at different temperatures. The wear rate of the SDCM-SS steel is lower than that of the H13 steel at each test temperature. The SDCM-SS steel has superior wear resistance compared with the H13 steel, especially at higher temperatures such as 600 and 700 °C. The wear rate of the SDCM-SS steel changes slightly as the temperature is varied; its value fluctuates from 0.57 to 1.01 $\times 10^{-8}$ mm^3/Nm. However, the H13 steel exhibits a greater wear rate under identical test parameters. The wear rate of the H13 steel is slightly greater than that of the SDCM-SS steel at 400 and 500 °C. When the ambient temperature rises to 600 and 700 °C, the H13 steel exhibits a very high wear rate; however, the wear rate of the SDCM-SS steel is still low. For both steels, the wear rate initially decreases and subsequently increases as the temperature is increased. The lowest wear rates for the SDCM-SS and H13 steels were recorded at 600 and 500 °C, respectively. These observations suggest that the two steels exhibit different wear mechanisms during sliding. Figure 8 presents the friction coefficient of the SDCM-SS and H13 steels as a function of the sliding period at various temperatures. In most cases, the SDCM-SS steel has a lower friction coefficient compared with that of the H13 steel. At

400 °C, the average friction coefficient values of the SDCM-SS and H13 steels are 0.47 and 0.58, respectively. The friction coefficient of the SDCM-SS steel is still lower than that of the H13 steel at 500 °C. At 600 °C, the two steels have similar average friction coefficients. However, at 700 °C, the average friction coefficient values of the SDCM-SS and H13 steels are 0.28 and 0.41, respectively.

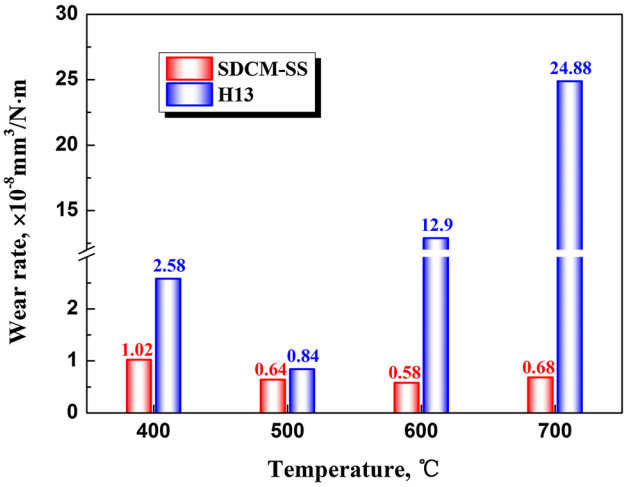

Fig. 7 Wear rate of SDCM-SS and H13 steel under different temperatures

Tribo-oxidation has an important role with regard to the friction behavior of steel, especially at high temperature (Ref 17, 23). Tribo-oxidation reduces the friction coefficient of the steel by forming a protective layer (Ref 17). The SDCM-SS steel has higher oxidizability, and therefore, results in more tribo-oxidation during sliding compared with the H13 steel, which has a greater Cr content (5.5%). Such tribo-oxidation can prevent adhesion between friction pairs and protect underlying materials from mechanical damage. Therefore, the wear rate and friction coefficient of SDCM-SS steel are lower than those of H13 steel.

3.5 Worn Surface and Subsurface

Figures 9 and 10 show the morphologies of the worn surfaces and subsurfaces of the SDCM-SS steel and H13 steel under various conditions. Tribo-oxides can be observed on the worn surfaces of both steels at all temperatures.

At 400 °C, the tribo-oxide layer covered the worn surface of the SDCM-SS steel. In certain areas, a patch-like tribo-oxide layer with a smooth surface exists on the worn surface, as

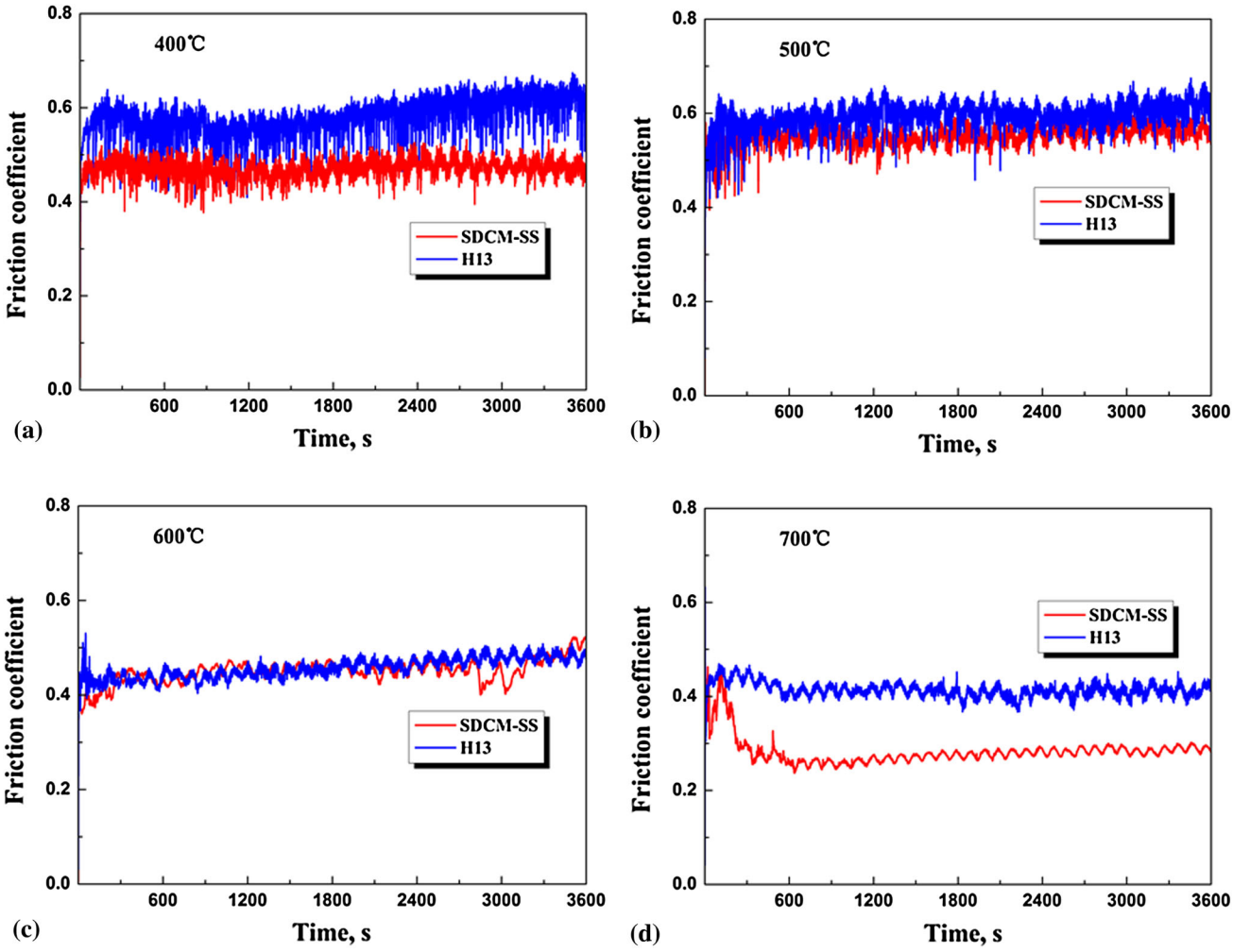

Fig. 8 Friction coefficient of tested steels at (a) 400 °C, (b) 500 °C, (c) 600 °C, and (d) 700 °C

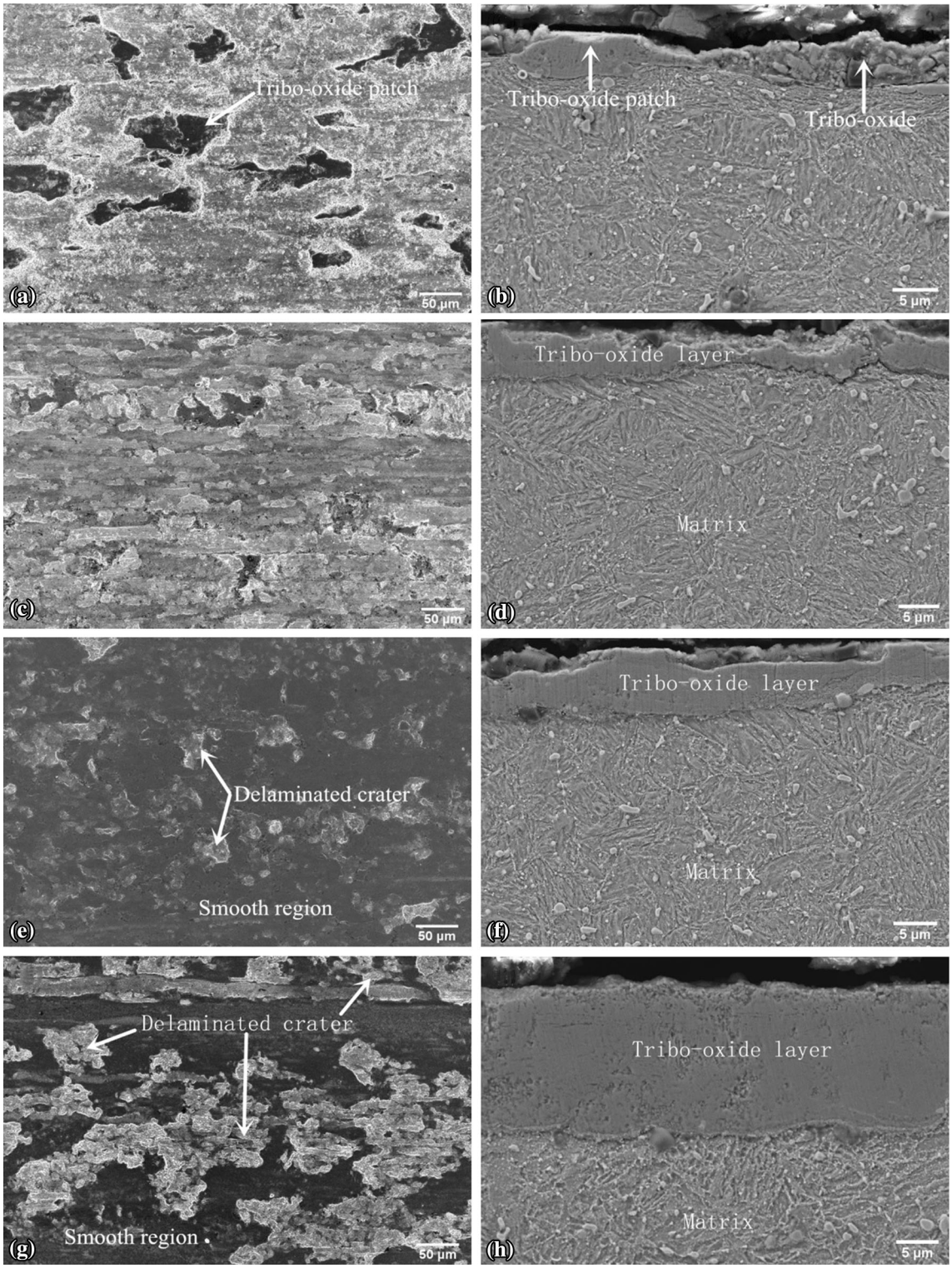

Fig. 9 The worn surface and subsurface of SDCM-SS steel at (a, b) 400 °C, (c, d) 500 °C, (e, f) 600 °C, and (g, h) 700 °C

shown in Fig. 9(a, b). Two types of oxide exist on the worn surface. One consists of a compact patch-like tribo-oxide layer (maximum thickness of 5.3 μm), and the other consists of areas (maximum thickness of 6.2 μm) formed by the assembly of compact oxide particles during the sliding process. Under the same conditions, the tribo-oxide patch on the worn surface of the H13 steel is smaller than that of the SDCM-SS steel, as shown in Fig. 10(a). Figure 10(b) shows that the size of the tribo-oxide patch (maximum thickness of 3.2 μm) of the H13 steel is smaller than that of the SDCM-SS steel.

The degree of tribo-oxidation increases as the temperature increases. Figure 9(c, d) shows that the worn surface of the

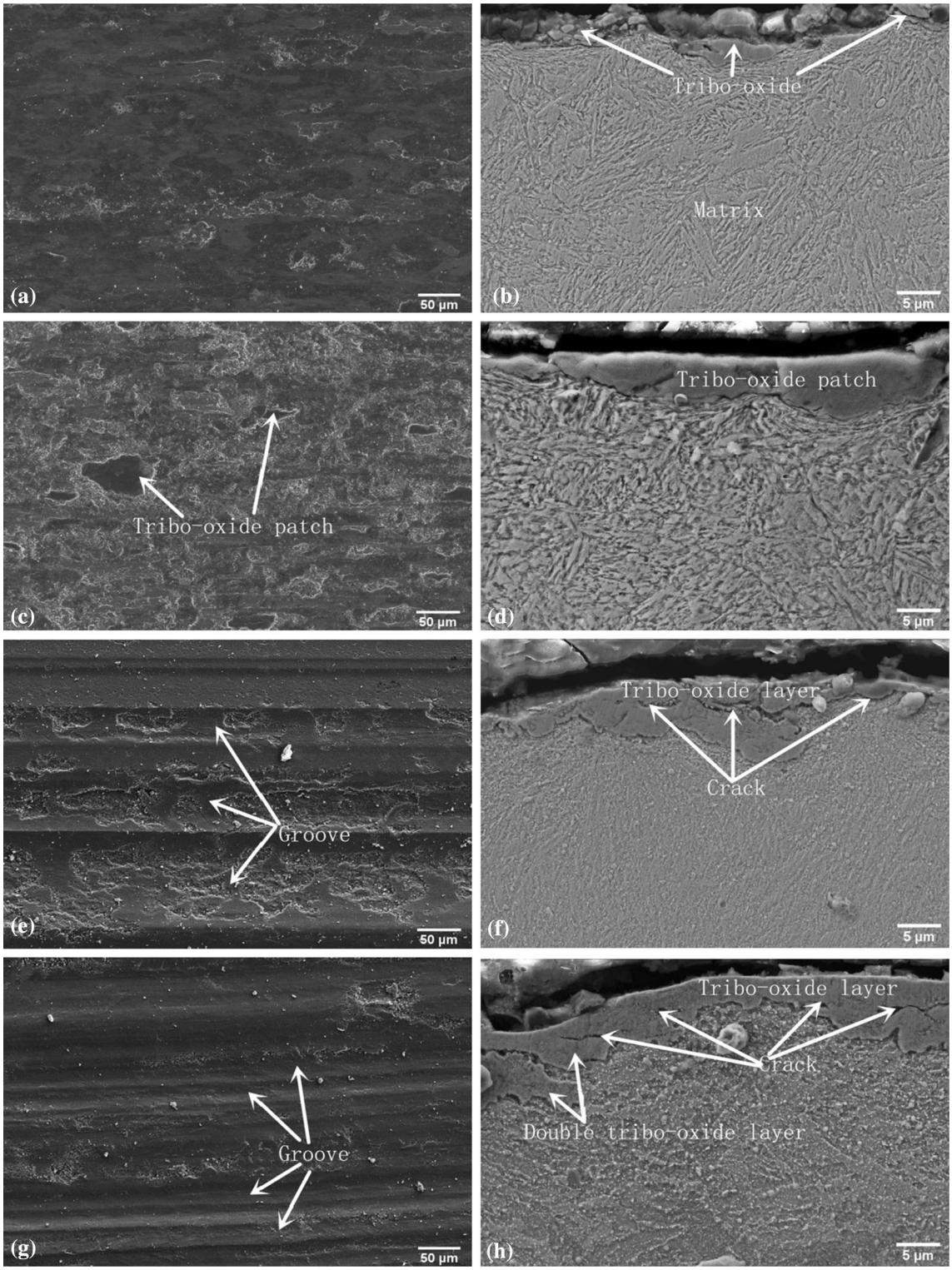

Fig. 10 The worn surface and subsurface of H13 steel at (a, b) 400 °C, (c, d) 500 °C, (e, f) 600 °C, and (g, h) 700 °C

SDCM-SS steel is entirely covered with a single tribo-oxide layer (thickness of 3.1-6.8 μm) at 500 °C. The morphology of the worn surface consists of smooth undelaminated and delaminated regions. The tribo-oxide layers tend to crack due to a fatigue mechanism and are likely to spall off during the sliding process; subsequently, wear debris and delaminated craters are generated on the worn surface. Stott et al. (Ref 1-3) investigated the relationship between sliding wear and high-temperature oxidation in super-alloys. They described the role of tribo-oxide layers, known as 'glazes,' which form on the sliding surfaces during frictional contact. Glazes can temporarily protect surfaces from further contact damage. If the glazes

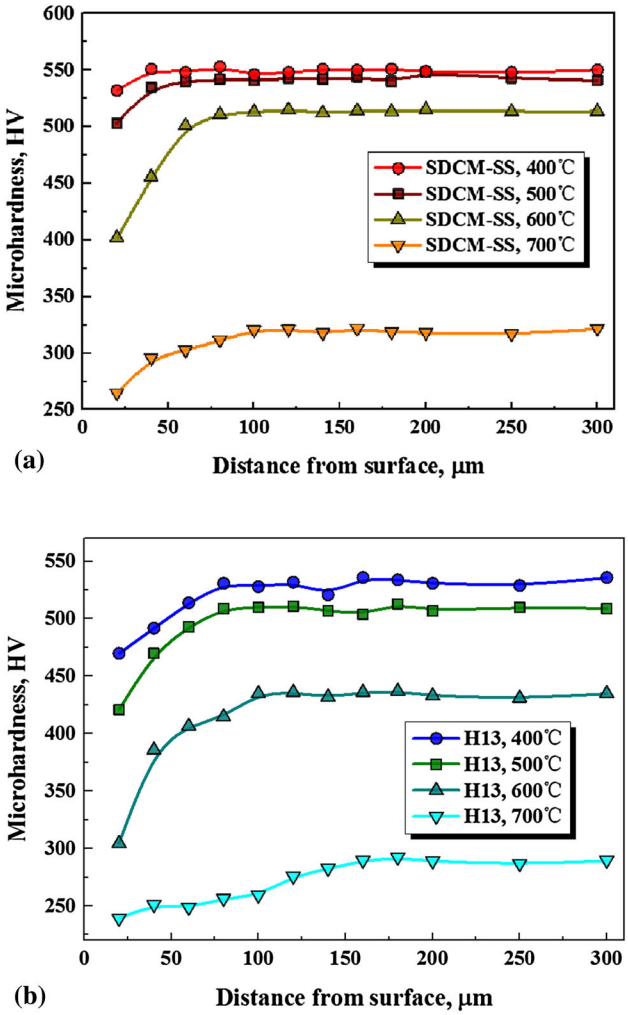

Fig. 11 Hardness distribution away from the worn surface of (a) SDCM-SS and (b) H13 steels

wear off, new glazes are formed to replace them. This progress of formation, loss, and reformation can result in short-term friction or wear transients. This phenomenon is similar to that associated with the friction coefficient in this work. Meanwhile, Fig. 10(c) and (d) shows that at 500 °C, the degree of tribo-oxidation on the worn surface of the H13 steel increases and a large tribo-oxide patch (maximum thickness of 7 μm) is formed.

Figure 9(e) shows that at 600 °C, the surface of the tribo-oxide layer is relatively smooth except for a few areas containing delaminated craters (white regions). Delamination of the tribo-oxide layer can cause wear loss during sliding. Figure 9(f) shows that a tribo-oxide layer, with a thickness of approximately 4.5-8.0 μm, entirely covers the worn surface of the SDCM-SS steel. However, under the same conditions, the morphology of the worn surface of the H13 steel obviously differs to that of the SDCM-SS steel. Although the tribo-oxide layer entirely covers the worn surfaces of both steels, the H13 steel has a higher wear rate. Figure 10(e) shows the presence of traces, with the appearance of valley-like grooves, on the worn surface. Figure 10(f) shows the appearance of many cracks in the tribo-oxide layer. Meanwhile, the thickness of the tribo-oxide layer varies from 1 to 9 μm and grows deeply into the matrix in some regions.

At 700 °C, the worn surface of the SDCM-SS steel is similar to that observed at 600 °C. However, at 700 °C, the size of the delaminated area (white area in Fig. 9(g)) is larger than that at 600 °C. Figure 9(h) shows that the thickness of the tribo-oxide layer further increases to 18 μm. The tribo-oxide layer of the SDCM-SS steel exhibited characteristics of a single layer, and no cracks formed between the tribo-oxide layer and matrix. Figure 10(g) and (h) presents the morphology of the worn surface of the H13 steel at 700 °C. The thickness of the tribo-oxide layer is between 2.6 and 10 μm. The tribo-oxide layer grows deeply into the matrix and forms a double tribo-oxide layer in some regions. Cracks are generated at the internal tribo-oxide layer and between the tribo-oxide layer and matrix.

Friction results in plastic deformation and frictional heat during sliding. The strain and temperature gradients cause dynamic changes in the microstructure and properties of the substructure, which affect the wear behavior (Ref 33). The frictional heating and high surrounding temperature generate a higher temperature on the worn surface, and consequently, the tribo-oxide layer beneath the substrate softens. The hardness distribution curves can reflect the softening of the subsurface matrix.

Figure 11 illustrates the microhardness distributions of the two steels following the experiments. The hardness decreases from the matrix toward the worn surface. Following sliding, the degree of reduction in hardness differs for the two steels. Following testing at temperatures of 400 and 500 °C, the hardness of the steel decreases to a certain extent; however, the matrices of both steels maintained a relatively high level of hardness. The matrices of the SDCM-SS and H13 steels had sufficient strength to effectively support the tribo-oxide layer, which can reduce the wear rate. In this case, the wear rate was governed by oxides that delaminated from within the tribo-oxide layer or at the interface between the tribo-oxide layer and substrate (Ref 16).

When the temperature was 600 °C, there was a significant decrease in the hardness of the H13 steel compared with that of the SDCM-SS steel. During sliding, there was a severe decease in the hardness of the H13 steel. The reduction in hardness consequently reduced the degree of support provided to the tribo-oxide layer, and therefore, cracks generated easily and propagated into the matrix. The cracks caused a great amount of oxide to peel from the tribo-oxide layer and matrix. Therefore, the wear rate significantly increased at 600 °C. On this occasion, the wear conditions were considered to be beyond those of mild oxidative wear. Wang et al. (Ref 10, 16, 19, 20) defined this type of wear mechanism as the transition from mild oxidative wear to severe oxidative wear. Owing to its high temper stability, the matrix of the SDCM-SS steel still maintained a high hardness of approximately 510 HV, as shown in Fig. 11(a). Marui et al. (Ref 9) indicated that under severe conditions, the wear rate was not primarily governed by the oxide layer; the wear behavior strongly depends on the reduction in hardness and the microstructural variation of the steel. The matrix of the SDCM-SS steel could still support the tribo-oxide layer under good conditions. Therefore, a relatively low wear rate was maintained for the SDCM-SS steel at 600 °C.

At 700 °C, there was a severe decrease in the hardness of both steel grades. A high degree of thermal softening and plastic deformation directly accelerates the delamination of the tribo-oxide. Figure 12(a) and (b) shows that the surrounding temperature and frictional heating accelerated the recovery of

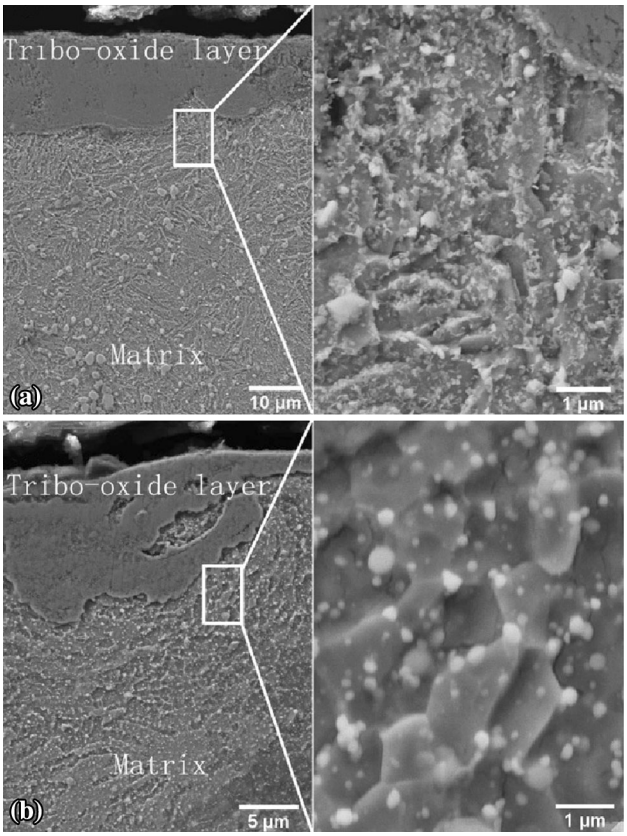

Fig. 12 The worn subsurface microstructure of (a) SDCM-SS and (b) H13 steels after wear test at 700 °C

the subsurface microstructure. For both steels, this resulted in an obvious decrease of the matrix hardness. The hardness of the SDCM-SS steel was still greater than that of the H13 steel. This is because many fine M_2C and VC secondary carbides precipitated during tempering, which can postpone the recovery process and the softening of the martensite microstructure, as described in section 3.2. Therefore, the SDCM-SS steel can maintain a higher hardness compared with the H13 steel. Figure 12(b) shows that significant recovery of the H13 steel occurred following the sliding test. The softened matrix tends to result in large plastic deformation; cracks are generated and propagate during sliding. As the cracks grow to a critical size, delamination of the matrix occurs, which results in a greater wear rate (Ref 34). Under these conditions, the oxide grows deeply into the matrix, forming a double tribo-oxide layer in some regions. Subsequently, cracks propagate to the inner tribo-oxide layer and between the tribo-oxide layer and matrix. Figure 13(b) shows the wear debris, with a large size, that formed because of such delamination. Therefore, the wear rate of the H13 steel seriously increased at temperatures above 600 °C. The hardness values of the subsurface and matrix of the SDCM-SS steel were greater than those of the H13 steel under the same conditions. Delamination only occurred at the internal tribo-oxide layer; as shown in Fig. 13(a), the wear debris has a relatively small size (about 2 μm). The supply of fine oxide particles to the wear surface reduced the friction coefficient and accelerated the transition from severe to mild oxidative wear (Ref 17). Fine oxide particles can reduce wear and friction by functioning as a solid lubricant. This explains why the friction coefficient of the SDCM-SS steel is obviously lower than that of the H13 steel at 700 °C.

3.6 Discussion of Wear Behavior and Mechanism

The high-temperature wear behaviors and mechanisms of the steels are closely related to the tribo-oxide and matrix (Ref 3, 10, 12, 13, 16, 20, 21). Tribo-oxidation leads to a reduction in the wear rate when the matrix has sufficient strength to support the tribo-oxide layer. If the matrix can maintain sufficient strength to provide support, the tribo-oxide layer will function as a protective layer against severe wear. In this case, the degree of reduced wear depends on the amount of tribo-oxide or thickness of the tribo-oxide layer. However, if the matrix, especially the substrate beneath the oxide layer, is not sufficiently strong to support the formation and maintenance of a single tribo-oxide layer, the occurrence of tribo-oxidation would not reduce wear.

The worn surfaces and subsurfaces were presented in various states and with different characteristics, which were related to the wear mechanism of the material (Ref 20). At different temperatures, the wear mechanisms can be clarified by thoroughly examining the morphology, composition, and structure of the worn surface and subsurface. Figures 9 and 10 show SEM images of the worn surface and subsurface morphologies. For both steels, at 400 °C, the existence of tribo-oxides could be observed within the morphological images of the worn surface and subsurface. It is clear that oxidative wear prevailed for both steels in this study; however, differences could be observed in the degree of tribo-oxidation and the size of the area covered by the tribo-oxide patch. The SDCM-SS steel, with high oxidizability, could form a greater amount of oxide compared with the H13 steel, as illustrated in section 3.3. Therefore, for the SDCM-SS steel, the degree of tribo-oxidation, as well as the area covered by the tribo-oxide patch, was greater. Meanwhile, the hardness of both steels was still high, as shown in Fig. 11. Sufficient strength was provided to support the tribo-oxide layer, which can reduce the wear rate. Under these conditions, the reduction in wear correlates with the degree of tribo-oxidation and thickness of the tribo-oxide layer. Therefore, the SDCM-SS steel had a lower wear rate and friction coefficient than the H13 steel at 400 °C.

The degree of tribo-oxidation increased as the surrounding temperature increased. Figure 9(c) and (d) shows that a single tribo-oxide layer completely covers the worn surface of the SDCM-SS steel at 500 °C. Due to a fatigue mechanism, the tribo-oxide layer would crack and subsequently spall off; this represents the physical process of wear loss and is defined as typical mild oxidative wear by Quinn (Ref 12, 13) and Wilson et al. (Ref 35). The wear rate decreased because of the presence of a single tribo-oxide layer. Wang et al. (Ref 36) found that mild oxidative wear prevailed when a single oxide layer reached a certain thickness and the degree of subsurface plastic deformation was low. The degree of tribo-oxidation of the H13 steel was lower than that of the SDCM-SS steel. However, the cover rate of the tribo-oxide patch increased compared with that at 400 °C. This explains why the wear rate of the H13 steel was at its lowest at 500 °C. The single tribo-oxide layer did not completely cover the worn surface, and therefore, the friction coefficient of the H13 steel was still higher than that of the SDCM-SS steel. The matrices of the two steel grades were still sufficiently hard under this condition. Therefore, the reduction in wear due to tribo-oxidation still depends on the degree of

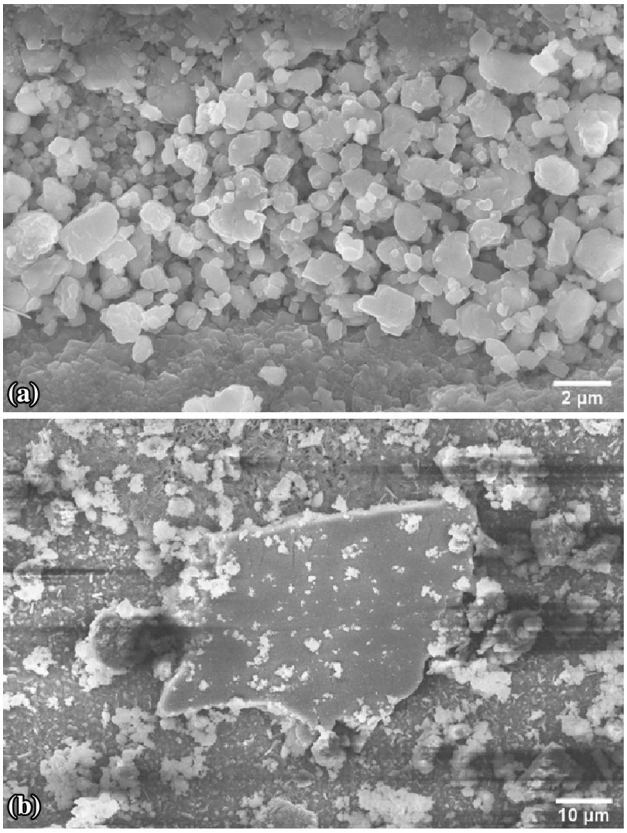

Fig. 13 Morphologies of wear debris of (a) SDCM-SS and (b) H13 steels at 700 °C

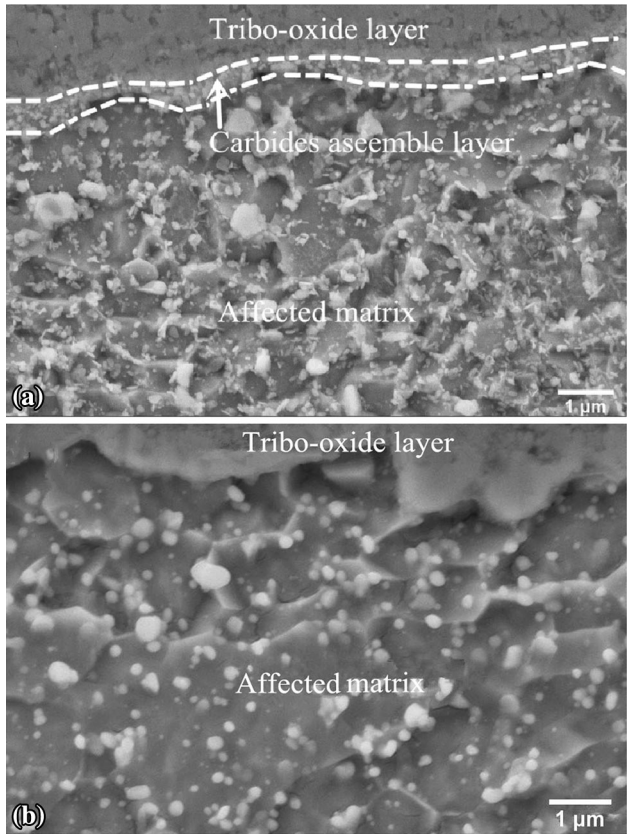

Fig. 14 Cross-section microstructure of worn surface and subsurface of (a) SDCM-SS and (b) H13 steels at 700 °C

tribo-oxidation and thickness of the tribo-oxide layer. The SDCM-SS steel, with high oxidizability, had greater wear resistance than the H13 steel at 500 °C.

When the temperature was 600 °C, a single tribo-oxide layer was preserved on the worn surface of the SDCM-SS steel, and a high hardness value was maintained, as shown in Fig. 9(f) and 11(a). In this case, mild oxidative wear prevailed. A thicker tribo-oxide layer formed on the worn surface and there was an increase in the proportion of areas consisting of a smooth surface. Therefore, there was a further decrease in the wear rate of the SDCM-SS steel at 600 °C. The tribo-oxide completely covered the worn surface of the H13 steel; however, its hardness significantly decreased at 600 °C, as shown in Fig. 10(f) and 11(b). Many cracks propagated into the inner surface and subsurface of the tribo-oxide layer. The thickness of the tribo-oxide layer was inhomogeneous and a double tribo-oxide layer formed during the sliding process. This type of oxidative wear differs from mild oxidative wear; it was referred to as a transition from mild to severe oxidative wear by previous researchers (Ref 10, 16, 19). It was reported that a harder matrix can support the tribo-oxide layer more effectively than a soft matrix (Ref 37). The SDCM-SS steel has superior temper stability performance at high temperature compared with the H13 steel. It is likely that the high temper stability ensures that the matrix has sufficient strength to support the formation of a defect-free tribo-oxide layer that can cover the entire worn surface. Under these conditions, the H13 steel presented severe oxidative wear; however, the SDCM-SS steel still exhibited mild oxidative wear. This explains why there was an obvious increase in the wear rate of the H13 steel when the temperature was 600 °C.

Figure 9(e) and (g) shows that for the SDCM-SS steel, the proportion of delaminated areas increases as the temperature increases; the wear rate also increased as the temperature was increased from 600 to 700 °C. In addition, observations of the cross-sections and morphologies of the worn surface and subsurface of the SDCM-SS steel revealed the existence of a single tribo-oxide layer on the worn surface. Therefore, a mild wear mechanism and low wear rate were still maintained for the SDCM-SS steel in this temperature region. There was a severe decrease in the hardness of the H13 steel at 700 °C, as shown in Fig. 11(b). The oxides grew deeply into the matrix, and a double tribo-oxide layer formed in some regions. Severe oxidative wear prevailed for the H13 steel under this condition.

It is important to study the subsurface microstructure of the SDCM-SS steel at 700 °C. Figure 14 shows the subsurface microstructure beneath the tribo-oxide layers of the two steels. There were many fine carbides in the subsurface matrix of the SDCM-SS steel. The hard second-phase particles are the most important parameter for determining the wear resistance of the steel. They can protect the matrix against wear (Ref 38). With regard to oxidative wear, the function of the carbides depends on their influence on the matrix. Secondary phases can affect the sliding wear by hardening the matrix. It can be observed that the microstructures differ for the SDCM-SS and H13 steels, as shown in Fig. 14(a) and (b). The cross-section of the worn surface of the H13 steel consisted of a tribo-oxide layer

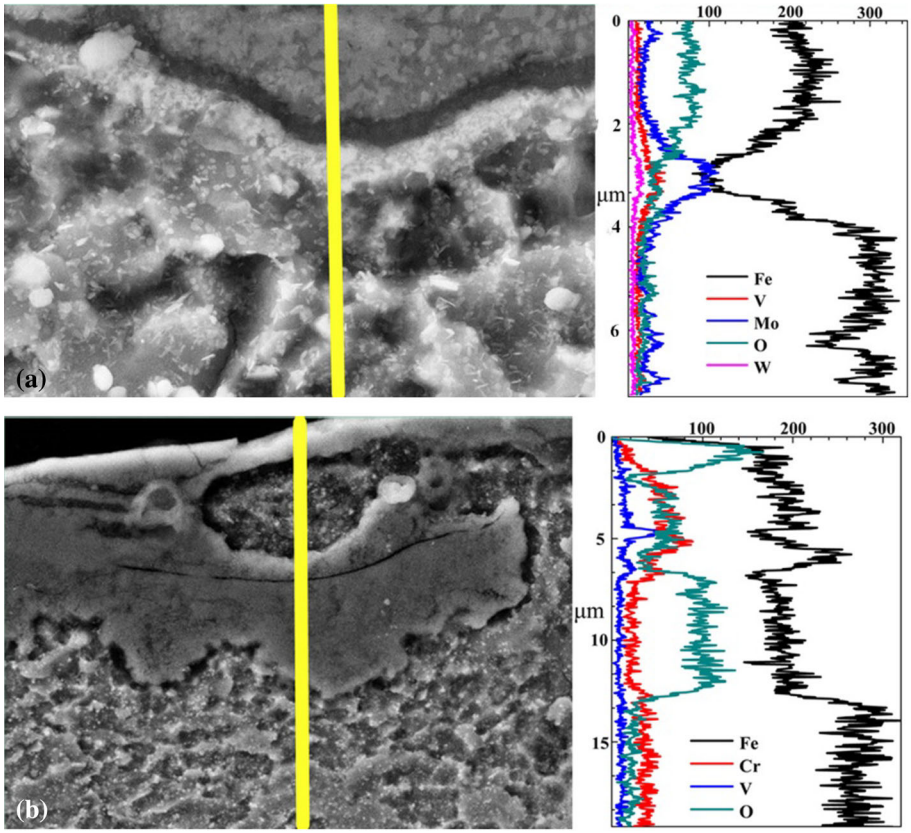

Fig. 15 EDS line-scan analysis on the cross-section of worn subsurface of (a) SDCM-SS and (b) H13 steels at 700 °C

and an affected matrix. However, an additional assembled carbide layer could be observed in the cross-section of the worn surface of the SDCM-SS steel, as shown in Fig. 14(a). Figure 15 shows the results of the energy dispersive x-ray spectrometry line scanning analysis performed on the cross-section of the worn subsurface. Figure 15(a) shows that the molybdenum and vanadium content of the assembled carbide layer was significantly higher than that of the matrix.

This layer may have formed via the aggregation of carbides during sliding. These carbides, defined in section 3.2, with high size stability and hardness, would support the tribo-oxide layer and impede the growth of oxides into the matrix. Meanwhile, these carbides have a strong cohesive bond with the metallic matrix and cannot be easily removed because this would cause delamination of the tribo-oxide layer. The high thermodynamic stability of these carbides can hinder further oxygen diffusion into matrix. Therefore, the assembled carbides can impede the growth of the tribo-oxide layer. Although the hardness of the SDCM-SS steel matrix at 700 °C is lower than that of the H13 steel at 600 °C, the assembled carbide layer can provide sufficient additional support for the formation and growth of a single thick tribo-oxide layer. Thus, at 700 °C, the SDCM-SS steel exhibits mild oxidative wear and a low wear rate with a single thick layer.

At 400 and 500 °C, both types of steel exhibited mild oxidative wear. The substrate had sufficient hardness to provide support to the tribo-oxide patch or layer, which can reduce the wear rate. The SDCM-SS steel has higher oxidizability; therefore, it can form more tribo-oxides during the sliding process compared with H13 steel. Therefore, the SDCM-SS steel has a lower wear rate and friction coefficient.

Owing to its high temper stability, the SDCM-SS steel maintained its high hardness at 600 °C, and therefore, the single tribo-oxide layer could be effectively supported. The wear rate further decreases as the tribo-oxide layer thickness and size of the areas with a smooth surface increase. However, the hardness of the H13 steel significantly decreased. This facilitated the generation and propagation of cracks within and beneath the tribo-oxide layer, which accelerated the delamination of the tribo-oxide layer. Consequently, conditions of mild oxidative wear were not maintained and severe oxidative wear occurred, which resulted in a high wear rate. A similar, but more severe phenomenon occurred for the H13 steel when the temperature increased to 700 °C.

At 700 °C, the SDCM-SS steel, with high temper stability, can still support the single tribo-oxide layer on the worn surface. The assembled carbide layer plays an important role under these conditions. The carbide layers improve the support provided to the tribo-oxide layer, obstruct the entry of oxygen into the matrix, and impede the growth of the tribo-oxide layer. Such factors ensure that the predominant wear mechanism of the SDCM-SS steel remains as mild oxidative wear. The wear resistance of the SDCM-SS steel is higher than that of the H13 steel at high temperature. This is owed to the particular oxidizability and temper stability of the SDCM-SS steel. The formation of many oxides, as well as the tribo-oxide layer, is facilitated during the sliding process because of the high oxidizability of the steel. The high-temperature temper stability

can help to maintain a certain strength and hardness, thus avoiding large plastic deformation and providing support to the tribo-oxide layer at high temperature. These factors postpone the transition from mild oxidative wear to severe wear.

4. Conclusions

(1) The SDCM-SS steel had greater tempering resistance and temper stability compared with the H13 steel. A great number of secondary carbides, Mo_2C and VC, precipitate during the tempering of the SDCM-SS steel, which shifts the secondary-hardening peak toward a higher temperature. These carbides, which have a greater size stability at high temperature, hinder the movement of dislocations and postpone the softening of martensite.

(2) The SDCM-SS steel has greater wear resistance compared with the H13 steel. The high oxidizability of the SDCM-SS steel facilitates the generation and growth of the tribo-oxide layer, which is maintained at high temperature because of the high temper stability of the steel. The combination of these two factors result in the high wear resistance of the SDCM-SS steel.

(3) The SDCM-SS steel, which exhibits high temper stability, maintains a certain strength and hardness, avoiding large plastic deformation and effectively supporting the tribo-oxide layer at high temperature. The high temper stability postpones the transition from mild to severe wear, and conditions of mild oxidative wear are maintained for long periods at high temperature. Mild oxidative wear is the predominant wear mechanism for the SDCM-SS steel between 400 and 700 °C.

Acknowledgments

This work supported by the National Natural Science Foundation of China (Grant Nos. 51401117 and 51171104). The authors would like to thank Na. Min from Instrumental Analysis and Research Center of Shanghai University for the help with the TEM measurements.

References

1. O. Barrau, C. Boher, R. Gras, and F. Rezai-Aria, Analysis of the Friction and Wear Behaviour of Hot Work Tool Steel for Forging, *Wear*, 2003, **255**, p 1444–1454
2. C. Boher, S. LeRoux, L. Penazzi, and C. Dessain, Experimental Investigation of the Tribological Behavior and Wear Mechanisms of Tool Steel Grades in Hot Stamping of a High-Strength Boron Steel, *Wear*, 2012, **294–295**, p 286–295
3. M.X. Wei, F. Wang, S.Q. Wang, and X.H. Cui, Comparative Research on the Elevated-Temperature Wear Resistance of a Cast Hot-Working Die Steel, *Mater. Des.*, 2009, **30**, p 3608–3614
4. G.A. Fontalvo and C. Mitterer, The Effect of Oxide-Forming Alloying Elements on the High Temperature Wear of a Hot Work Steel, *Wear*, 2005, **258**, p 1491–1499
5. P.J. Blau, Elevated-Temperature Tribology of Metallic Materials, *Tribol. Int.*, 2010, **43**, p 1203–1208
6. M. Pellizzari, D. Cescato, and M.G. DeFlora, Hot Friction and Wear Behaviour of High Speed Steel and High Chromium Iron for Rolls, *Wear*, 2009, **267**, p 467–475
7. S. Hernandez, J. Hardell, H. Winkelmann, M.R. Ripoll, and B. Prakash, Influence of Temperature on Abrasive Wear of Boron Steel and Hot Forming Tool Steels, *Wear*, 2015, **338–339**, p 27–35
8. X.H. Cui, S.Q. Wang, F. Wang, and K.M. Chen, Research on Oxidation Wear Mechanism of the Cast Steels, *Wear*, 2008, **265**, p 468–476
9. E. Marui, N. Hasegawa, H. Endo, K. Tanaka, and T. Hattori, Research on the Wear Characteristics of Hypereutectoid Steel, *Wear*, 1997, **205**, p 186–199
10. S.Q. Wang, M.X. Wei, F. Wang, and Y.T. Zhao, Transition of Elevated-Temperature Wear Mechanisms and the Oxidative Delamination Wear in Hot-Working Die Steels, *Tribol. Int.*, 2010, **43**, p 577–584
11. F.H. Stott, J. Glascott, and G.C. Wood, Factors Affecting the Progressive Development of Wear-Protective Oxides on Iron-Base Alloys During Sliding at Elevated Temperatures, *Wear*, 1984, **97**, p 93–106
12. T.F.J. Quinn, Review of Oxidational Wear Part I: The Origins of Oxidational Wear, *Tribol. Int.*, 1983, **16**, p 257–271
13. T.F.J. Quinn, Review of Oxidational Wear part II: Recent Developments and Future Trends in Oxidational Wear Research, *Tribol. Int.*, 1983, **16**, p 305–315
14. J. Archard., W. Hirst, The wear of metals under unlubricated conditions, *Proceedings of the Royal Society A: Mathematical, Physical and Engineering Sciences*, 1956, p 397–410
15. S.M. Hsu, M.C. Shen, and A.W. Ruff, Wear Prediction for Metals, *Tribol. Int.*, 1997, **30**, p 377–383
16. S.Q. Wang, L. Wang, Y.T. Wang, Y. Sun, and Z.R. Yang, Mild-to-Severe Wear Transition and Transition Region of Oxidative Wear in Steels, *Wear*, 2013, **306**, p 311–320
17. H. Kato, Severe-Mild Wear Transition by Supply of Oxide Particles on Sliding Surface, *Wear*, 2003, **255**, p 426–429
18. C.C. Viáfara and A. Sinatora, Influence of Hardness of the Harder Body on Wear Regime Transition in a Sliding Pair of Steels, *Wear*, 2009, **267**, p 425–432
19. S.Q. Wang, M.X. Wei, F. Wang, X.H. Cui, and C. Dong, Transition of Mild Wear to Severe Wear in Oxidative Wear of H21 Steel, *Tribol. Lett.*, 2008, **32**, p 67–72
20. S.Q. Wang, M.X. Wei, and Y.T. Zhao, Effects of the Tribo-Oxide and Matrix on Dry Sliding Wear Characteristics and Mechanisms of a Cast Steel, *Wear*, 2010, **269**, p 424–434
21. S.C. Lim, The Relevance of Wear-Mechanism Maps to Mild-Oxidational Wear, *Tribol. Int.*, 2002, **35**, p 717–723
22. A.W. Batchelor, G.W. Stachowiak, and A. Cameron, The Relationship Between Oxide Films and the Wear of Steels, *Wear*, 1986, **113**, p 203–223
23. F.H. Stott, The Role of Oxidation in the Wear of Alloys, *Tribol. Int.*, 1998, **31**, p 61–71
24. G. Straffelini, D. Trabucco, and A. Molinari, Oxidative Wear of Heat-Treated Steels, *Wear*, 2001, **250**, p 485–491
25. Q.Y. Zhang, K.M. Chen, L. Wang, X.H. Cui, and S.Q. Wang, Characteristics of Oxidative Wear and Oxidative Mildwear, *Tribol. Int.*, 2013, **61**, p 214–223
26. S.Q. Wang, F. Wang, K. Chen, and X.H. Cui, A Newly-Developed High Wear Resistant Cast Hot-Forging Die Steel, *ISIJ Int.*, 2007, **47**, p 1335–1340
27. N. Mebarki, D. Delagnes, P. Lamesle, F. Delmas, and C. Levaillant, Relationship Between Microstructure and Mechanical Properties of A 5% Cr Tempered Martensitic Tool Steel, *Mater. Sci. Eng. A*, 2004, **387–389**, p 171–175
28. Q.C. Zhou, X.C. Wu, N.N. Shi, J.W. Li, and N. Min, Microstructure Evolution and Kinetic Analysis of DM Hot-Work Die Steels During Tempering, *Mater. Sci. Eng. A*, 2011, **528**, p 5696–5700
29. P. Michaud, D. Delagnes, P. Lamesle, M.H. Mathon, and C. Levaillant, The Effect of the Addition of Alloying Elements on Carbide Precipitation and Mechanical Properties in 5% Chromium Martensitic Steels, *Acta Mater.*, 2007, **55**, p 4877–4889
30. A. Medvedeva, J. Bergström, S. Gunnarsson, and J. Andersson, High-Temperature Properties and Microstructural Stability of Hot-Work Tool Steels, *Mater. Sci. Eng. A*, 2009, **523**, p 39–46
31. M.X. Wei, S.Q. Wang, K.M. Chen, and X.H. Cui, Relations Between Oxidative Wear and Cr Content of Steels, *Wear*, 2011, **272**, p 110–121
32. F.H. Stott and G.C. Wood, The Influence of Oxides on the Friction and Wear of Alloys, *Tribol. Int.*, 1978, **11**, p 211–218

33. Y. Wang, T. Lei, and J. Liu, Tribo-Metallographic Behavior of High Carbon Steels in Dry Sliding: III. Dynamic Microstructural Changes and Wear, *Wear*, 1999, **231**, p 20–37
34. V. Abouei, H. Saghafian, and S. Kheirandish, Effect of Microstructure on The Oxidative Wear Behavior of Plain Carbon Steel, *Wear*, 2007, **262**, p 1225–1231
35. J.L. Sullivan, T.F.J. Quinn, and D.M. Rowson, Developments in the Oxidational Theory of Mild Wear, *Tribol. Int.*, 1980, **13**, p 153–158
36. M.X. Wei, S.Q. Wang, L. Wang, X.H. Cui, and K.M. Chen, Effect of Tempering Conditions on Wear Resistance in Various Wear Mechanisms of H13 Steel, *Tribol. Int.*, 2011, **44**, p 898–905
37. N. Saka, J.J. Pamies-Teixeira, and N.P. Suh, Wear of Two-Phase Metals, *Wear*, 1977, **44**, p 77–86
38. M. Vardavoulias, The Role of Hard Second Phases in the Mild Oxidational Wear Mechanism of High-Speed Steel-Based Materials, *Wear*, 1994, **173**, p 105–114